Inter-model variability and biases of the global water cycle in CMIP3 coupled climate models

2012 Environ. Res. Lett. 7 014006

(http://iopscience.iop.org/1748-9326/7/1/014006)

Environ. Res. Lett. **7** (2012) 014006 (12pp) doi:10.1088/1748-9326/7/1/014006

Inter-model variability and biases of the global water cycle in CMIP3 coupled climate models

Beate G Liepert[1] **and Michael Previdi**[2]

[1] NorthWest Research Associates, 4118 148th Avenue NE, Redmond, WA 98052, USA
[2] Lamont-Doherty Earth Observatory of Columbia University, 61 Route 9W, Palisades, NY 10964, USA
E-mail: Liepert@nwra.com

Received 26 September 2011
Accepted for publication 15 December 2011
Published 12 January 2012
Online at stacks.iop.org/ERL/7/014006

Abstract
Observed changes such as increasing global temperatures and the intensification of the global water cycle in the 20th century are robust results of coupled general circulation models (CGCMs). In spite of these successes, model-to-model variability and biases that are small in first order climate responses, however, have considerable implications for climate predictability especially when multi-model means are used. We show that most climate simulations of the 20th and 21st century A2 scenario performed with CMIP3 (Coupled Model Inter-comparison Project Phase 3) models have deficiencies in simulating the global atmospheric moisture balance. Large biases of only a few models (some biases reach the simulated global precipitation changes in the 20th and 21st centuries) affect the multi-model mean global moisture budget. An imbalanced flux of -0.14 Sv exists while the multi-model median imbalance is only -0.02 Sv. Moreover, for most models the detected imbalance changes over time. As a consequence, in 13 of the 18 CMIP3 models examined, global annual mean precipitation exceeds global evaporation, indicating that there should be a 'leaking' of moisture from the atmosphere whereas for the remaining five models a 'flooding' is implied. Nonetheless, in all models, the actual atmospheric moisture content and its variability correctly increases during the course of the 20th and 21st centuries. These discrepancies therefore imply an unphysical and hence 'ghost' sink/source of atmospheric moisture in the models whose atmospheres flood/leak. The ghost source/sink of moisture can also be regarded as atmospheric latent heating/cooling and hence as positive/negative perturbation of the atmospheric energy budget or non-radiative forcing in the range of -1 to $+6$ W m^{-2} (median $+0.1$ W m^{-2}). The inter-model variability of the global atmospheric moisture transport from oceans to land areas, which impacts the terrestrial water cycle, is also quite high and ranges from 0.26 to 1.78 Sv. In the 21st century this transport to land increases by about 5% per century with a model-to-model range from 1 to 13%. We suggest that this variability is weakly correlated to the land–sea contrast in air temperature change of these models. Spatially heterogeneous forcings such as aerosols contribute to the variability in moisture transport, at least in one model. The polewards shifts of dry zones in climate simulations of the 21st century are also assessed. It is shown that the multi-model means of the two subsets of models with negative and positive imbalances in the atmospheric moisture budget produce spatial variability in the dry zone positions similar in size to the spatial shifts expected from 21st century global warming. Thus, the selection of models also affects the multi-model mean dry zone

extension. In general, we caution the use of multi-model means of $E - P$ fields and suggest self-consistency tests for climate models.

Keywords: global water cycle, climate model validation, atmospheric moisture convergence, ghost forcing, climate predictions, dry zones

1. Introduction

As understanding of the Earth's climate system increased substantially over the years, modeling of climate also progressed rapidly. Observed changes such as increasing global temperatures and the intensification of the water cycle are now common, robust features of coupled general circulation models (CGCMs) as described in the 4th Assessment Report of the Intergovernmental Panel on Climate Change (IPCC-AR4). Due to these consistencies between models and observations, CGCMs are used more and more to predict other complex climate responses of natural and anthropogenic perturbations. Such responses are for example shifts in the edge of the dry zones. Model-to-model variability that may appear small in first order effects may, however have unexpected implications for more complex responses. Lucarini *et al* (2008) investigated future changes in the hydrology of the Danube Basin with CMIP3 CGCMs and discovered significant discrepancies in model predictions for this important transition region. Reichler and Kim (2008) suggested as approach to overcome model uncertainty the combination of atmospheric variables and models. They showed that multi-model means of combined variables of climate simulations represent the best estimates of the climate state when compared to 20th century observations. Their analysis was performed with data from the CMIP3 archive. Calculating multi-model means of simulations and multi-model means of subsets of simulations became a common approach in recent years. Climate forcings such as ozone recovery, and their climate responses were studied with multi-model means of hierarchies of models (e.g., Son *et al* 2008). Although, with this approach a few outlier models may be able to significantly skew outcomes and may result in misleading conclusions. Another issue in predicting future climate and source of prediction uncertainty originates from model evaluations with 20th century observations that may not necessarily represent future responses and be prone to uncertainty itself. Hence tests that are designed independently of observations and observational uncertainty are preferable.

Arguably the largest uncertainty in both climate observations and models arises from the hydrological cycle. While the basic processes are well known and the acceleration of the water cycle with global warming is well studied, the inter-model variability of variables describing hydrological processes remains high (Liepert and Previdi 2009). Here we investigate these inter-model variability and biases of the global water cycle in CMIP3 models. We focus on the atmospheric branch of the hydrological cycle because of its intrinsic connection to the energy budget of the atmosphere and thus to climate forcings and feedbacks (see e.g. Liepert 2010). Although the atmospheric moisture content is by far the smallest storage term in the global water cycle, even small variations can play key roles in the energy balance of the planet. Latent heating redistributes energy in the vertical column and cloud formation affects the emission of infrared and reflection of solar radiation while water vapor absorbs near-infrared and infrared radiation (e.g., Hansen *et al* 1997 and Previdi and Liepert 2011). The atmospheric moisture transport from oceans to land constitutes the moisture input to the continental freshwater cycle. Hence reliable climate impact assessments require accurately predicted atmospheric 'oceans to land' moisture transport. Another important predictor of the atmospheric moisture balance is the boundary of the dry zones on Earth defined as the spatial distribution of the zero net fluxes of precipitation and evaporation. This study investigates these processes as well. Described in section 2 is CMIP3 model data and data handling, and in section 3 the analysis of biases of the global atmospheric moisture balance in climate models including its implications. Inter-model variability of atmospheric moisture transport from oceans to land and variability of extensions of dry zones are discussed in sections 4 and 5.

2. Climate modeling data

The climate modeling experiments analyzed here are the archived CMIP3 simulations of fully coupled ocean–atmosphere general circulation models. Investigated are the 20th century scenarios with climate forcings determined by the individual modeling groups, and the 21st century scenario A2. Data from all runs of 18 models were downloaded from the archive (www-pcmdi.llnl.gov/ipcc/ipcc_data_status.php). The 21st century runs were available for only 16 of the 18 models. The data sets of the 20th and the 21st century were combined into one time series. The models are listed in table 1 and the abbreviations that follow the IPCC-AR4 nomenclature are in the note of table 1. For the atmospheric moisture balance analysis we examined ensemble means of all runs for each model and one arbitrary chosen run for each model. There were no differences in outcomes of the ensemble means versus the individual runs. Hence all results presented here are based on the analysis of individual model runs. For one model the analysis was performed with daily as well as monthly data. The finer temporal resolution did not change the outcome and hence monthly datasets are used in this study. All datasets for each model are processed in the spatial resolution provided by the modeling groups and archived in CMIP3. No re-gridding was necessary for this analysis except for the calculation of the multi-model mean dry zone distributions. Available column integrated data were obtained from the archive and no vertical integration was performed, except one model that

Table 1. Global annual means, inter-annual variability and linear trends of residuals of the atmospheric moisture balance Res $= (E - P - \frac{\partial W}{\partial t})$ as described in (3) for CMIP3 climate models. Listed are global annual means and standard deviations for the model time series of the 20th and 21st scenario A2. Also listed are global precipitation (P) trends and the percentage of residual (Res) trend to precipitation (P) trend for the same simulations. The excess latent heating that corresponds to the moisture imbalance is given in W m^{-2}. Models with flux correction are marked with *, no cloud ice data available **, and models without cloud ice/*water* data are marked with ***. (Note: BCCR-BCM2.0, 2005 Bjerknes Centre for Climate Research, Norway. CCSM3, 2005 National Center for Atmospheric Research, USA. CGCM3.1(T47), 2005 Canadian Centre for Climate Modeling and Analysis, Canada. CNRM-CM3, 2004 Météo-France/Centre National de Recherches Météorologiques, France. CSIRO-MK3.0, 2001 Commonwealth Scientific and Industrial Research Organization (CSIRO) Atmospheric Research, Australia. ECHAM5/MPI-OM, 2005 Max Planck Institute for Meteorology, Germany. ECHO-G, 2004 Meteorological Institute of the University of Bonn, Germany. FGOALS-g1.0, 2004 National Key Laboratory of Numerical Modeling for Atmospheric Sciences and Geophysical Fluid Dynamics (LASG)/Institute of Atmospheric Physics, China. GFDL-CM2.0, 2005 US Department of Commerce/National Oceanic and Atmospheric Administration (NOAA)/Geophysical Fluid Dynamics Laboratory (GFDL), USA. GISS-EH, 2004 NASA/GISS, USA. GISS-ER, 2004 NASA/GISS, USA. INM-CM3.0, 2004 Institute for Numerical Mathematics, Russia. IPSL-CM4, 2005 Institut Pierre Simon Laplace, France. MIROC3.2(medres), 2004 Center for Climate System Research (University of Tokyo), National Institute for Environmental Studies, and Frontier Research Center for Global Change (JAMSTEC), Japan. MRI-CGCM2.3.2, 2003 Meteorological Research Institute, Japan. PCM, 1998 National Center for Atmospheric Research, USA. UKMO-HadCM3, 1997 Hadley Centre for Climate Prediction and Research/Met Office, UK. UKMO-HadGEM1, 2004 Hadley Centre for Climate Prediction and Research/Met Office, UK.)

CMIP3 Model*	Mean ± Std. dev. Res $= (E - P - \frac{\partial W}{\partial t})$ (Sv)	Trend Res $= (E-P-\frac{\partial W}{\partial t})$ (Sv/100 yr)	Trend P (Sv/100 yr)	Trend Res/trend P (%)	Excess latent heat (W m^{-2})
BCCR-BCM2.0	−0.453 ± 0.010	−0.010	0.41	−2.44	−2.22
CCSM3	−0.018 ± 0.006	−0.000	0.53	−0.06	−0.09
CGCM3.1(T47)*	−0.005 ± 0.005	−0.002	0.53	−0.36	−0.03
CNRM-CM3	−0.752 ± 0.013	−0.027	0.48	−5.51	−3.69
CSIRO-MK3.0	0.007 ± 0.006	0.004	0.28	1.52	0.03
ECHAM5-MPI-OM	−0.053 ± 0.007	−0.001	0.40	−0.16	−0.26
ECHO-G**	0.053 ± 0.006	0.006	0.20	2.93	0.26
FGOALS-g1.0	−1.339 ± 0.020	−0.044	−0.02	199.19	−6.56
GFDL-CM2.0	0.014 ± 0.005	−0.005	0.16	−3.34	0.07
GISS-EH	−0.013 ± 0.004	−0.000	−0.02	0.38	−0.06
GISS-ER	−0.022 ± 0.004	0.001	0.36	0.29	−0.11
INM-CM3.0*	−0.065 ± 0.005	0.007	0.66	1.07	−0.32
IPSL-CM4	0.198 ± 0.005	−0.007	0.56	−1.25	0.97
MIROC3.2(medres)	−0.019 ± 0.006	−0.001	0.09	−1.16	−0.09
MRI-CGCM2.3.2***	−0.079 ± 0.009	0.009	0.50	1.84	−0.39
PCM (NCAR)***	−0.022 ± 0.005	0.001	0.40	0.18	−0.11
UKMO-HadCM3	0.003 ± 0.005	−0.000	0.25	−0.08	0.02
UKMO-HadGEM1	−0.017 ± 0.005	0.000	0.09	0.22	−0.09
Mean	−0.136 ± 0.009	−0.004	0.32	—	−0.70
Median	−0.018 ± 0.006	−0.000	0.38	—	−0.09

did not provide column integrated water vapor for the archive (see table 1). Individual model land masks were used for the calculation of the ocean to land atmospheric moisture transport. In case of models with mixed land–ocean grid cells, cells with land areas over 50% were considered land cells. The spatial integration was performed by summation of grid cell values, after multiplication with the calculated rectangular grid cell areas.

The variables that were obtained are monthly means of surface latent heat flux and monthly mean precipitation rates for each model. Precipitation consists of solid and liquid fluxes including negative values for dew and frost. Ocean evaporation was calculated from the available surface latent heat flux divided by the latent heat of vaporization ($L_{\text{vap}} = 2501$ J g^{-1}). Sublimation of sea ice was calculated from the surface latent heat flux over sea ice divided by the latent heat of sublimation ($L_{\text{sub}} = 2835$ J g^{-1}). Evapo-transpiration and sublimation over land was calculated from the surface latent heat flux divided by the latent heat of vaporization ($L_{\text{vap}} = 2501$ J g^{-1}). This procedure slightly overestimates sublimation rates over land ice and snow because latent heat of vaporization is slightly smaller than latent heat of sublimation. Snow/ice coverage over land was not available for all models. For one model we calculated land sublimation explicitly over ice and snow with the latent heat of sublimation and did not find accountable discrepancies after global integration. In the following we will use the expression 'evaporation' for the sum of evapo-transpiration, evaporation and sublimation. From the CMIP3 archive we further obtained the archived monthly means of column integrated water vapor for each model. For most models column integrated cloud liquid and ice water content was also available (marked in table 1). The solid and liquid contributions to total atmospheric moisture are small compared to the contribution in the gas phase. Atmospheric moisture content was calculated as the sum of solid, liquid water, and water vapor.

3. Global atmospheric moisture balance

3.1. Method

According to Peixoto and Oort (1992) the moisture balance of an atmospheric column can be described in its vertically

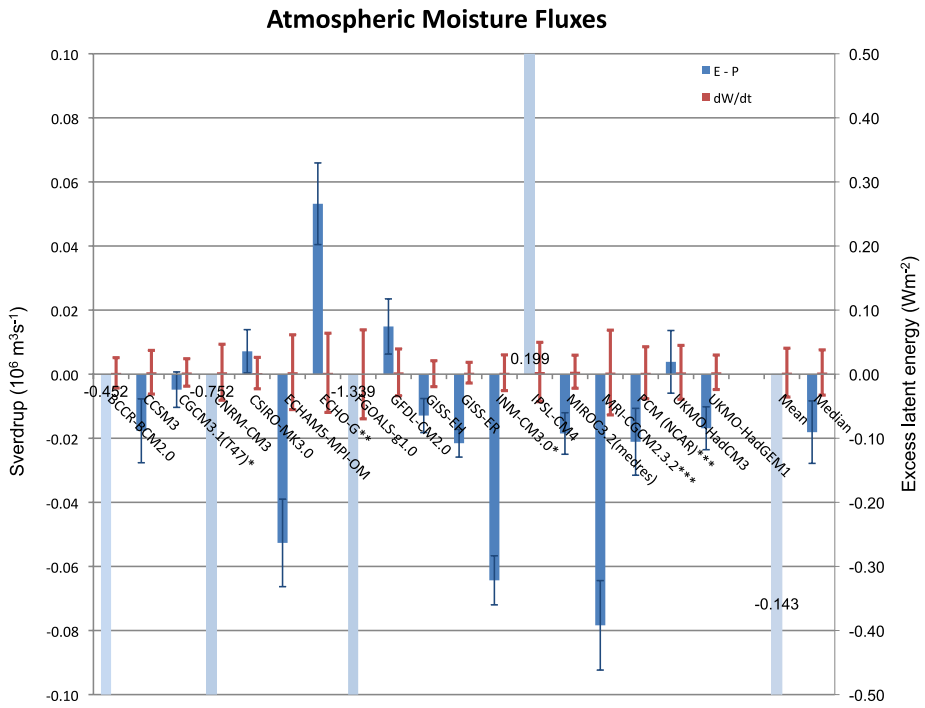

Figure 1. Global atmospheric moisture fluxes $E - P$ in blue and moisture content change in red for CMIP3 climate models. Shown are long-term annual means in columns and standard deviations in error bars. The calculations were performed with the time series of the 20th and 21st scenarios A2. The light blue columns are too large to be shown but the corresponding values are given on the column. Note that models with flux correction are marked with *, without cloud ice with **, and without cloud ice and water with ***.

integrated form as follows:

$$\frac{\partial W}{\partial t} + \vec{\nabla}_h \cdot \vec{Q} = E - P$$

$$\text{with } \vec{Q} = \int_{z=0}^{\infty} \vec{v} q \, \mathrm{d}z \qquad W = \int_{z=0}^{\infty} q \, \mathrm{d}z. \tag{1}$$

The vector $\vec{v}$ is the horizontal wind velocity and q the atmospheric moisture content (vapor, liquid, solid) of the vertical layer dz. When integrated over the globe, the horizontal moisture divergence $\vec{\nabla}_h \cdot \vec{Q}$ in the atmospheric column disappears. The column integrated atmospheric moisture storage change $\frac{\partial W}{\partial t}$ is then balanced by the sources and sinks of atmospheric moisture, which are the surface fluxes of evaporation minus precipitation $E - P$. Furthermore, when applied to temporally discrete data indexed 'i', the global atmospheric moisture gain or loss within the time period of n time steps can be described by the net accumulation of sources E_i and sinks P_i as noted on the right side of (2):

$$\frac{\partial W}{\partial t} = E - P \Rightarrow \langle W_n - W_1 \rangle = \sum_{i=1}^{n} \langle E_i - P_i \rangle. \tag{2}$$

This implies that the global mean of the atmospheric moisture content changes balances the net fluxes in and out of the atmosphere. Applied to monthly modeling data (2) requires that the annual atmospheric moisture gains/losses (e.g., from January to December or any other 12-month period) are balanced by the yearlong net accumulation of monthly E_i minus P_i.

$$\text{Res} = E - P - \frac{\partial W}{\partial t} \Rightarrow \text{Res}(y)$$

$$\equiv \sum_{i=1}^{12} \langle E_i - P_i \rangle - \langle W_{12} - W_1 \rangle. \tag{3}$$

Thus for the annual atmospheric moisture budget, a potential residual or imbalance Res for the year y can be calculated and a time series of these annual residuals can be constructed after (3).

3.2. Results

Figure 1 summarizes 20th–21st century long-term annual means and inter-annual variability of the two components of the atmospheric moisture balance on the left side of (3) for each CMIP3 model. The inter-annual variability in all cases is calculated as standard deviation of the annual means after the linear trends of the data records were removed. This procedure seems appropriate for most models (see figure 2) albeit the estimates might be too high for the few models with large non-linear inter-annual trends. We discuss these models in more detail below. The units for all moisture fluxes considered here are given in Sverdrup (1 Sverdrup = 1 Sv = 10^6 m^3 s^{-1} = 31.6 × 10^{12} m^3 a^{-1}).

Illustrated in figure 1 in red error bars is the inter-annual variability of the time series of $\frac{\partial W}{\partial t}$. Not recognizable in figure 1 are the mean annual atmospheric moisture changes. The long-term multi-model mean of moisture change within a

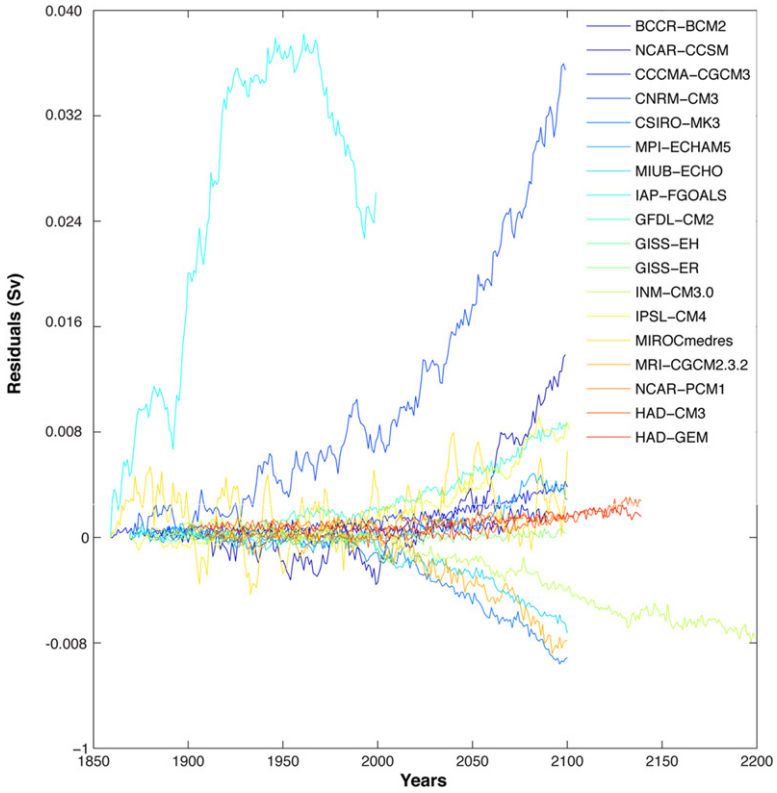

Figure 2. Global atmospheric moisture imbalances in CMIP3 climate models. Shown are time series of annual mean residuals for the 20th and 21st scenarios A2 combined. The initial imbalances were removed from the time series. The residuals are given in Sverdrup.

year is 0.000 48 Sv. A positive, albeit small, increase like this is expected due to the increasing moisture-holding capacity of the atmosphere with global warming. An increase in global atmospheric moisture content W of about 3.03×10^{12} m^3 over the 200 yr period can be calculated from the multi-model mean of these data. These changes in atmospheric moisture content and content variability are small compared to other storage terms of the water cycle. Nonetheless the atmospheric moisture increases are important in the climate system because they initiate the radiative water vapor and cloud feedbacks (Previdi 2010).

Also shown in figure 1 are the long-term annual means of the time series of $E - P$ in columns and their inter-annual variability in error bars, both in blue. Mean $E - P$ values exceed the actual variability of moisture storage changes $\frac{\partial W}{\partial t}$ (red error bars) in almost all models and hence result in unbalanced moisture budgets (3). The analysis was repeated with all available simulations and no differences in the results were obtained. As mentioned before, the original data are only multiplied with grid cell areas before summation. Hence it is unlikely that numerical errors from the integration can cause these residuals. Also mentioned in section 2 are missing cloud ice water content data for some models as well as the treatment of land sublimation as evaporation. We further tested the possible biases due to these uncertainties with one model that includes all data records. Omitting these data sets could not account for the observed deficiencies.

The long-term means, inter-annual variability and long-term trends of the residuals are also listed in table 1. As pointed out in table 1 some models balance the atmospheric moisture budget. For example the model CGCM3.1 (T47), which is flux corrected (marked with '*' in table 1), closes the atmospheric moisture budget, while other models (CSIRO-MK3.0 and UKMO-HadCM3) that are without flux adjustments are also in closure within the uncertainty range (information on flux adjustments was taken from IPCC-AR4 2007 table 8.1). Positive biases could be identified for five and negative biases for thirteen models. Negative $E - P$ values in table 1 and figure 1 indicate, 'leaking' of moisture from the atmospheres, and positive $E - P$ values indicate, 'flooding' of model atmospheres. The multi-model mean is negative with -0.14 Sv and therefore models tend to 'leak' on average. The residuals are generally small compared to the calculated global annual mean precipitation trends in the 20th and 21st century (table 1). Nonetheless, the unphysical multi-model mean leaking is about one third the size of the multi-model mean precipitation trend (table 1). This is the case because, for a few models, the biases are so large that they can reach the magnitude of the inter-annual variability of precipitation. Consequently the more appropriate multi-model median of the residuals is calculated, which is significantly smaller with -0.02 Sv. It is important to point out that the leaking or flooding of the atmosphere that is anticipated based on the global imbalances of E and P, is not reflected in the actually simulated atmospheric moisture content W and its inter-annual variation $\frac{\partial W}{\partial t}$ as discussed above and shown in figure 1. In the flooding models, the actually simulated moisture content changes $\frac{\partial W}{\partial t}$ are significantly smaller than

would be expected from the modeled $E - P$, while in the leaking models the simulated increases of $\frac{\partial W}{\partial t}$ are smaller and of opposite sign than expected from the modeled $E-P$ values. This result therefore implies the appearance of an artificial or unphysical source of atmospheric moisture in the models that leak and an unphysical sink in the models that flood.

In general the global atmospheric moisture imbalances are small compared to precipitation and other fluxes in the global water cycle. They are also not unexpected in climate models (see e.g., Rodríguez *et al* 2011 and Kavetski and Clark 2010). These small biases in atmospheric moisture however, become important if we consider them as perturbation of the atmospheric energy budget. Additional moisture translates into excessive latent heat release into the atmosphere through phase transition in precipitation formation (see also Edwards 2007). The atmosphere responds to this 'ghost' latent heating with various feedback processes, which cannot be identified easily. Hence the artificial source of moisture can be interpreted as 'instantaneous', non-radiative forcing in the atmospheric energy budget. Table 1 lists for each model the 'excess latent heat' added to the atmosphere, which are in the range of -1 to $+6$ W m^{-2} with a small positive multi-model median of $+0.1$ W m^{-2}. This result is in line with Lucarini and Ragone (2011) who derived an energetic imbalance of the atmosphere between -1 and $+3$ W m^{-2} in CMIP3 models for the pre-industrial control runs.

In contrast to energetic imbalances, climate predictions of water cycle strengths are not necessarily influenced by biases, because considered in climate model analyses are often differences of two climate states in energetic equilibrium or changes over time from a control run. Changes over time (drifts) of these biases on the other hand, would influence climate predictions of water cycle strength. Tendencies of biases in each model, calculated as linear trends for the annual residuals are listed in table 1. We chose a linear trend analysis for simplicity reason albeit some drifts appear of higher order (figure 2). As consequence the calculated linear trends of the time series should be considered as first order estimates. In general the analysis reveals positive and negative drifts of the residuals in most models as illustrated in figure 2 (the initial imbalance of each run is removed). The drifts are by and large negligible compared to global precipitation trends (see table 1). Although for some models, the trends in the residuals can be as large as 5% of predicted precipitation changes and in one climate model the bias drift reaches twice the precipitation trend of the 100 yr period. Consequently multi-model means of global precipitation trends should be considered with caution and multi-model medians should be calculated instead.

4. Global atmospheric moisture transport from oceans to land

4.1. Method

The net atmospheric moisture transport from oceans to land connects ocean fresh water cycle and land hydrology and is hence a crucial parameter in climate impact studies and applications. Continental runoff, which is not explicitly investigated here constitutes the return flow and eventually closes the global water cycle. Atmospheric moisture transport is commonly calculated as atmospheric moisture convergence with three-dimensional wind and moisture fields (1). Because of the potentially high uncertainty in numerical precision in directly calculating vertically integrated convergence, we chose the more indirect atmospheric moisture budget approach (see also Lucarini *et al* 2008). The atmospheric moisture supply for all land areas is derived from the moisture budget over the oceans.

$$\oiint_{\partial Oc} \mathrm{d}\vec{S} \cdot \vec{Q} = \iiint_{Oc} \vec{\nabla}_h \cdot \vec{Q}\, \mathrm{d}V$$
$$= \iiint_{Oc} \left(E - P - \frac{\partial W}{\partial t} \right) \mathrm{d}V. \quad (4)$$

The left side of (4) describes the integration of Gauss's flux theorem. Horizontal moisture flux $\vec{Q}$ through the surfaces $\mathrm{d}\vec{S}$ of the atmospheric columns over the oceans is equal to the moisture convergence in the volumes $\mathrm{d}V$ of the atmospheric columns over the oceans. This is the case because fluxes through the air–sea boundary are E and P while the fluxes at the top of the atmosphere are expected to be zero. The moisture convergence can then be replaced by the atmospheric moisture budget of (1). The globally integrated formulation of the atmospheric moisture transport from oceans to land is therefore:

$$\iint_{\partial Oc} \mathrm{d}\vec{S} \cdot \vec{Q} = \left\langle -\frac{\partial W}{\partial t} + E - P \right\rangle_{Oc}. \quad (5)$$

The brackets $\langle\,\rangle_{Oc}$ symbolize the integration of all columns over the ocean areas. Time series of annual atmospheric moisture transports from oceans to land can now be calculated for all CMIP3 climate models using (5).

4.2. Results

As indicated in table 2 the long-term average atmospheric moisture transport from oceans to land varies quite significantly from model-to-model with a range from 0.26 to 1.78 Sv. The multi-model mean of 1.1 Sv and median of 1.2 Sv for the 20th and 21st century simulations however, remain close to the observational estimate of 1.2 Sv (e.g., Baumgartner and Reichel 1975). The inter-annual variability (calculated as standard deviation after the record was linearly detrended) is on average about 5–6% of the total transport in the models. In CMIP3 models, a significant portion of the long-term variability stems from underlying trends toward increasing moisture transport to land areas. The linear trends in moisture transports from oceans to land areas in the 20th and 21st century are shown in figure 3. Overall, land areas will receive on average about 0.04–0.05 Sv (about 4%) more moisture per 100 yr through atmospheric transport. This average increase amounts to an extra moisture input to land of about the size of the discharge of the River Nile in hundred years (e.g., Gupta 2007). In the models CCSM3 and ECHO-G, the intensified moisture transports reach up to 0.13 Sv in

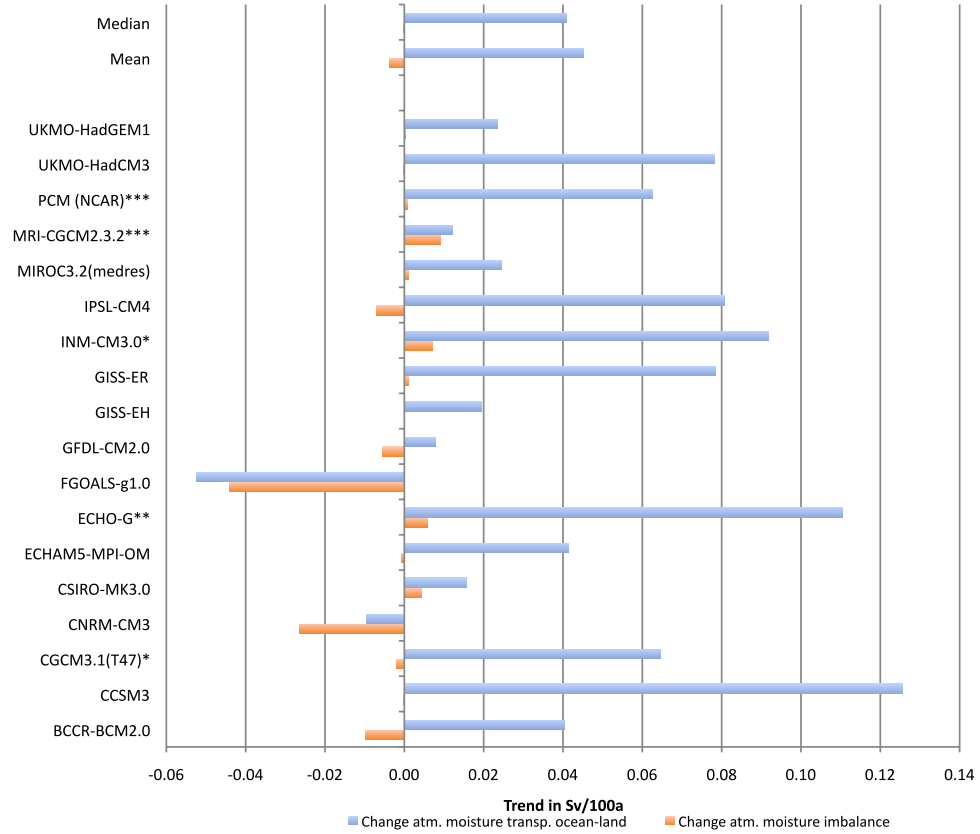

Figure 3. Simulated future changes in global atmospheric moisture transport from ocean to land for CMIP3 climate models. Shown are linear trends of annual mean moisture transport in blue bars and linear trends of annual mean residuals in the atmospheric moisture budgets in orange bars. The calculations were performed with the combined time series of the 20th and 21st (A2) century scenarios.

Table 2. Global annual means, inter-annual variability and linear trends of atmospheric moisture transport from ocean to land areas as described in (5) for CMIP3 climate models. Listed are global annual means and standard deviations for the model time series of the combined 20th and 21st scenario A2. Further listed is the area of the dry zones as fractions of the area of the globe for the first 20 yr period of the 21st century scenario A2. The difference in global area fraction of the dry zones between the first (2001–20) and the last (2081–2100) 20 yr periods are also listed. Models written in *italic* have positive biases in their atmospheric moisture balance (flooding models).

CMIP3 Model	Mean ± std. dev. atm. moisture transport ocean–land (Sv)	Trend atm. moisture transport ocean–land (Sv/100 yr)	Mean (2001–20) global dry zone area fraction	Difference (2001–20)–(2081–2100) global dry zone area fraction
BCCR-BCM2.0	1.01 ± 0.04	0.04	0.406	−0.005
CCSM3	1.44 ± 0.05	0.13	0.391	−0.002
CGCM3.1(T47)*	1.32 ± 0.04	0.06	0.406	−0.002
CNRM-CM3	0.55 ± 0.05	−0.01	0.385	−0.006
CSIRO-MK3.0	*1.02 ± 0.04*	*0.02*	*0.411*	*−0.005*
ECHAM5-MPI-OM	0.96 ± 0.05	0.04	0.395	−0.030
*ECHO-G***	*1.21 ± 0.06*	*0.11*	*0.365*	*0.009*
FGOALS-g1.0	0.26 ± 0.06	−0.05	No data	No data
GFDL-CM2.0	*1.25 ± 0.06*	*0.01*	*0.403*	*−0.012*
GISS-EH	1.18 ± 0.03	0.02	No data	No data
GISS-ER	1.78 ± 0.05	0.08	0.398	−0.011
INM-CM3.0*	1.11 ± 0.05	0.09	0.404	0.008
IPSL-CM4	*1.44 ± 0.04*	*0.08*	*0.409*	*0.007*
MIROC3.2(medres)	1.20 ± 0.07	0.02	0.378	0.012
MRI-CGCM2.3.2***	1.29 ± 0.12	0.01	0.401	0.004
PCM (NCAR)***	1.12 ± 0.04	0.06	0.442	0.001
UKMO-HadCM3	*1.25 ± 0.06*	*0.08*	*0.391*	*−0.004*
UKMO-HadGEM1	1.27 ± 0.06	0.02	0.417	−0.008
Mean	1.15 ± 0.07	0.05	0.400	−0.002
Median	1.21 ± 0.06	0.04	0.403	−0.006

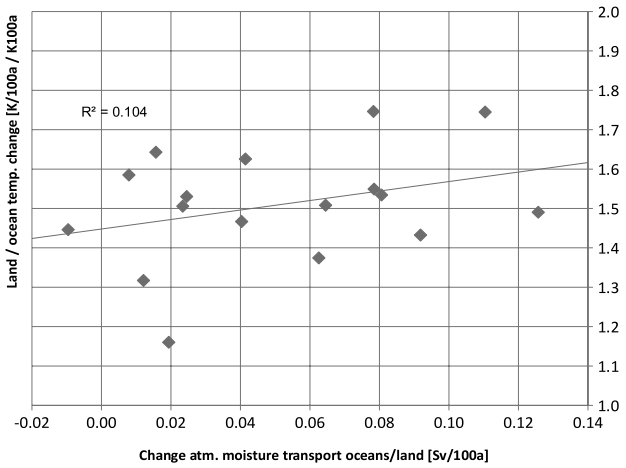

Figure 4. Changes in global atmospheric moisture transport from ocean to land versus ratio of ocean–land near surface temperature changes calculated for each CMIP3 climate model. The calculations were performed with the combined time series of the 20th and 21st (A2) century scenarios. The model results of FGOALS-g1.0 were removed from the analysis.

100 yr or an increase of 10% of the total atmospheric, ocean to land transport.

Further shown in figure 3 are the linear trends of the residuals of the atmospheric moisture balances of simulations of the 20th and 21st centuries (table 1). In figure 3 the two models (CNRM-CM3 and FGOALS-g1.0) with reduced atmospheric moisture transport are also the models with strong increasing artificial leaking from model atmospheres. The median of the drifts in atmospheric moisture balances is coincidently zero due to compensation amongst models. We suspect that drifts in the atmospheric moisture imbalance affect the atmospheric moisture transport from oceans to land areas because the largest flux in the global water cycle is ocean evaporation. For most models however, the trends in the global residuals are small compared to the trends in atmospheric moisture transport (see multi-model mean and median in figure 3). The atmospheric moisture transport from ocean to land redistributes energy and thus reduces the ocean–land temperature contrast. In climate change context this atmospheric bridge can therefore be correlated to the temperature change contrast between land and ocean. Figure 4 illustrates as a scatter plot the regression of atmospheric moisture transport changes from ocean to land and air temperature changes of ocean versus land for the CMIP3 model scenarios of the 20th and 21st century. There is indeed a weak correlation of $R^2 = 0.10$ of temperature change contrasts and moisture flux changes amongst the models. More detailed analyses are currently in process and will be published in the future.

5. Extension of the dry zone edges

5.1. Method

Several approaches exist for identifying the edges of the dry zones in the subtropics (see Seidel *et al* 2008 for an overview). For example, the descending branch of the Hadley circulation determines the edges of the subsidence region, which can be identified as the position of the jet streams or the zero net flow of mass from north to south in the lower atmosphere. Other distinct characteristics such as the stratospheric Brewer–Dobson circulation realized in the stratospheric ozone distribution or the tropopause height identify the width of the tropics and hence the edges of the dry zones as well. The ascending branch of the Hadley cell also produces cloud bands whose edges mark the beginning of the dry zone. The gradient of outgoing long-wave radiation is used for this approach. At the surface, dry zones are regions with evaporation exceeding precipitation and the edges are the contour line of $E - P = 0$ or $E = P$. This definition has been used in observations and modeling studies (see e.g., Previdi and Liepert 2007).

5.2. Results

Figure 5(a) shows the $E - P = 0$ contours for all CMIP3 models in light blue or light red color. Models with negative residuals in the moisture budget are marked in red and with positive residuals in blue. The inter-model variability of the position of the dry zones is large. Dry zone edges in bold colors represent the mean positions of the multi-model composites of the two model subsets with artificially leaking atmospheres is in bold red and artificially flooding in bold blue. As illustrated in figure 5(a) the different positions between the multi-model means of the subsets are minor compared to the inter-model spread and rarely systematic. Although some features are recognizable such as the reduced areal extend of the dry zones in Africa and Australia in the leaking model composite (bold red). Differences in the Eastern Pacific Walker circulation are also revealed with a zonal stretched dry zone edge of the descending branch in the tropical Pacific in the flooding model composite (bold blue) compared to the leaking subset. This pattern indicates a more pronounced double ITCZ for the models that experience positive biases. Overall, the model-to-model variability remains dominant.

In a former study (Previdi and Liepert 2007) we found as a robust result of all CMIP3 models the pole-ward extensions of the dry zone edges of about 1° of latitude with 21st century global warming. Here the formerly published pole-ward extensions are reproduced for the CMIP3 models. The spatial distributions of the dry zone edges of each model of the first 20 yr period in blue and the last 20 yr period of the 21st century in green are shown in figure 5(b). The contours of the multi-model means of these two time intervals are plotted in bold blue for the first and bold green for the last two decades. The inter-model variability of the dry zone edges for the predictions is again quite large and the shifts in dry zone edges in the 21st century as identified by the bold lines are similarly difficult to distinguish as the means of the two subsets in the climate models with different biases. The differences and shifts may be clearer shown as zonal averages, because of the latitudinal structures of $E - P$ fields. Zonal averaging was performed as follows: grid cell values with precipitation >

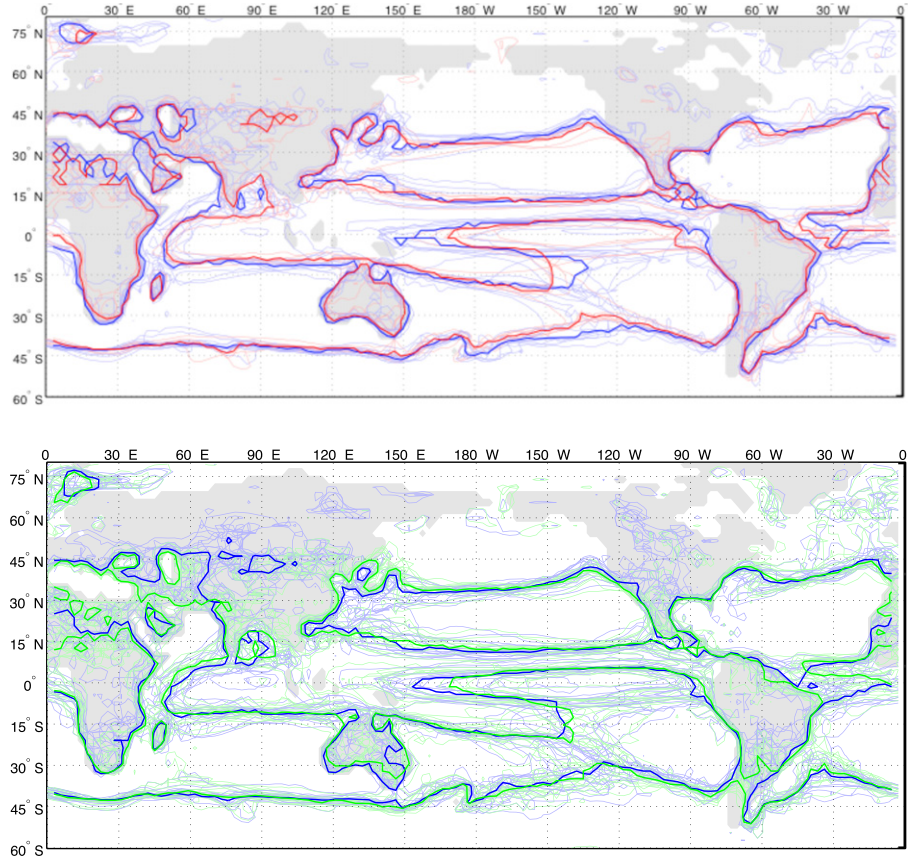

Figure 5. Predicted long-term mean positions of dry zone edges of the 21st century (A2) scenario for CMIP3 climate models. (Top) 21st century multi-model means for two subsets of models. In red are the contours of models with artificial leaking (globally negative atmospheric moisture imbalance) and in blue with artificial flooding of the atmospheres (globally positive atmospheric moisture imbalance). (Bottom) 21st century multi-model means for two 20 yr periods. In green are the contours of the dry zone edges from the means of the last two (2081–2100) and in blue for the first two decades (2001–20). Shown are the contour lines of balanced atmospheric moisture budget, which corresponds to $E - P = 0$, where evaporation equals precipitation. The thick contour lines represent the multi-model composites of dry zone edges of the corresponding subsets and time periods, while the thin lines represent results of individual models.

evaporation ('wet' cells) were set to the discrete value '−1' and grid cell values with evaporation ≥ precipitation ('dry' cells) were set to '+1'. These fields of discrete values were then zonal averaged for each model. A zonal average of −1 means dry zones are outside this latitude band.

The statistical analysis performed on these zonal dry zone edges are shown for the subsets of leaking (blue) and flooding models (red) at the top of figure 6, and for the first (blue) and last (green) two decades of the 21st century at the bottom of figure 6. There is significant overlap of the 25–75 percentiles for the bias subsets and time intervals in each latitude band. This means, due to the large model-to-model variability the shift in the dry zones and the differences between subsets of positive and negative imbalance models cannot be properly identified even in the zonal average.

We repeat the analysis for the combination of the negative and positive residual subsets and the two 20 yr time intervals of the 21st century predictions of the models. In this illustration of figure 7 only the multi-model means of the following subsets are plotted. The first and the last 20 yr period of the averages of the leaking models are in solid and dashed lines, shown in red, and the first and last 20 yr period of the flooding models are shown in solid (2001–20) and dashed (2081–2100) lines shown in blue. The differences between the first and the last 20 yr periods are similar for the two model subsets. The mean dry zone edge shifts slightly southward on the pole-ward side of the SH dry zone (around 40°S). Both NH dry zone edges also shift south (equator-ward) in the 21st century (solid to dashed lines). Nonetheless this result is overshadowed by the significant inter-model variability identified in the bias subsets of figure 7. Therefore we suggest using other atmospheric parameters described above for identifying shifting dry zones in climate models.

We further calculate the areal extent of the dry zones as fraction of the total area of the globe, which indicates whether the dry zones are shrinking or expanding. The areal fractions in table 2 reveal no significant differences between the two model subsets. The dry zones cover on average about 40% of the globe in these models. The calculation is repeated with the 21st century scenario experiments. The differences in areal sizes of the dry zones between the first two and the last two decades of the 21st century project no significant tendencies. In ten models the dry zones shrink slightly and in six models an equally small extension (less than 1%) is calculated. The models with negative or positive net moisture budgets do not show any preference for shrinking or expanding either. The

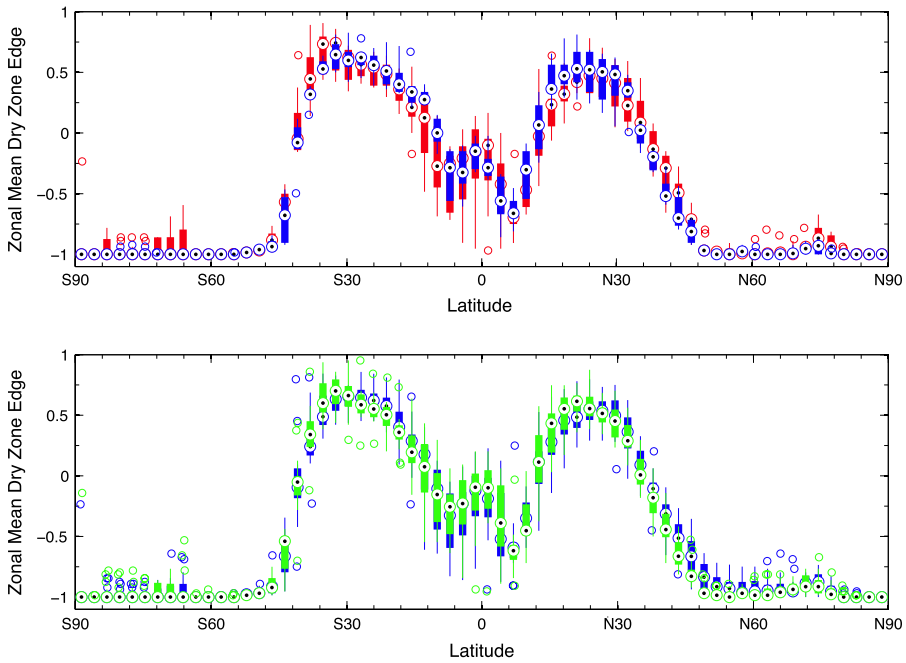

Figure 6. Statistics of the zonal mean positions of CMIP3 multi-model dry zone edges. (Top) Results for the subsets of artificially leaking (globally negative atmospheric moisture imbalance) models in red and flooding (globally positive atmospheric moisture imbalance) models in blue; (bottom) results of the first (in blue) and last (in green) 20 yr periods of the 21st century A2 scenario. The zonal means are calculated for the atmospheric moisture budgets, with value '−1' set for grid boxes where $E < P$, and value '+1' set $E \geq P$. The boxes represent the 25–75 percentile, the whiskers the range, the open circles the outliers and the black dotted circles the medians of the model spread for each latitude band.

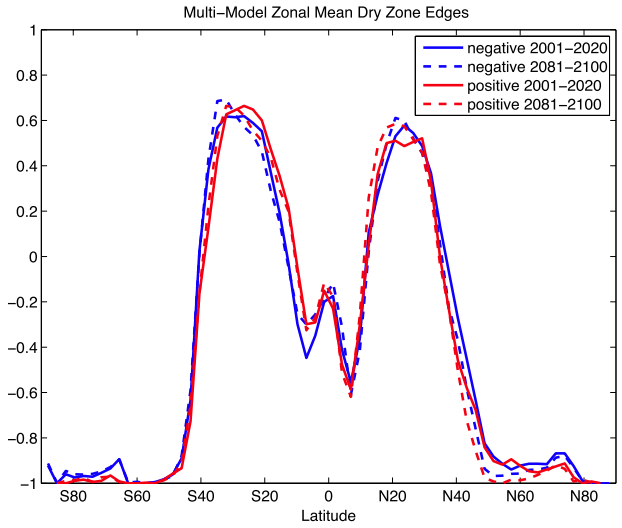

Figure 7. Zonal mean positions of CMIP3 multi-model mean dry zone edges of the first (full line) and last (dashed line) 20 yr periods of the 21st century A2 scenario. The multi-model means are separated into subsets of artificially leaking (globally negative atmospheric moisture imbalance) models in red and flooding (globally positive atmospheric moisture imbalance) models in blue. The zonal means are calculated for the atmospheric moisture budgets, with value '−1' set for grid boxes where $E < P$, and value '+1' for $E \geq P$.

areal extent analysis is hence inconclusive and in line with the zonal analysis. In general, the areal fraction of the dry zones seems a robust feature of the climate system similar to the global mean relative humidity.

6. Discussion and conclusions

In this study we assessed global atmospheric moisture budgets in CMIP3 climate model simulations of the 20th and 21st century scenario A2. For these models Reichler and Kim (2008) showed that for combinations of atmospheric variables the multi-model means represent the best estimates of the climate state when compared to 20th century observations. Based on our investigations, we suggest that for water cycle variables like precipitation or the $E - P$ field however, a few models can bias multi-model means considerably. Hence we propose the general use of medians for calculating multi-model averages. This is concluded from the global atmospheric moisture budget, which is out of balance by −0.14 Sv in the multi-model mean whereas the multi-model median is only out of balance by −0.02 Sv. The discrepancies in the moisture balances vary hugely amongst models and range from −1.34 to 0.20 Sv. The biases are also not constant over time and can drift significantly. Positive and negative drifts were detected for the simulations of the 20th and 21st century. The trends in the model biases range from less than a tenth of a per cent of simulated global precipitation trends to a few per cent. For one model the trend in the bias is 200% of the predicted precipitation change in a 100 yr period. Hence we suggest closure tests should be performed and models with large drifts should be excluded from multi-model average calculations.

The global biases in moisture balance can also be regarded as artificial 'leaking' of moisture from the atmosphere when the imbalances are negative (which is the

case in thirteen of the eighteen models). This leaking is artificial in the sense that the actual moisture content of the atmosphere is simulated to increase during the 20th and 21st centuries. Thus, discrepancies between the simulated $\frac{\partial W}{\partial t}$ and $E - P$ implies an unphysical, 'ghost' source of moisture. This 'ghost' moisture source can also be described as excess latent heating of the atmosphere and therefore as energy perturbation or non-radiative 'ghost' forcing. The excess latent heating ranges from -1 to $+6$ W m^{-2}, with a small multi-model median of $+0.1$ W m^{-2}. By calculating the global energy budget directly, Lucarini and Ragone (2011) identify imbalances of the atmospheric energy budget of similar magnitude (-1 to 3 W m^{-2}) in pre-industrial runs of CMIP3 models. They link these unphysical energy sinks or sources to the fact that kinetic energy dissipation by various processes is not accounted for in most GCMs. Kinetic processes mentioned are viscosity and diffusion, cloud parameterization and boundary layer interactions. It is worth noting that radiative forcings of non-CO_2 greenhouse gases are in the same size range and provoke considerable feedback mechanisms.

The model-to-model variability of atmospheric moisture transport from oceans to land is quite high and ranges from 0.26 to 1.78 Sv in CMIP3 simulations, while the inter-annual standard deviations are around 0.06 Sv in the 20th and 21st century scenarios. The global flux is 1.2 ± 0.3 Sv in the multi-model median, which matches observations quite well (Baumgartner and Reichel 1975, Schanze *et al* 2010). The changes over the 100 yr time period are all positive (except the two models with strongly drifting moisture imbalances). Based on our study we expect that land areas receive on average about 4% more moisture or 0.08 Sv in the 21st century. This is about a third of the observed drainage of a major river such as the Lena in Siberia that has an annual runoff of 0.17 Sv (see e.g., Gupta 2007). The variation of moisture transport is weakly correlated with the land–sea contrast of air temperature change. In general, the models with higher temperature change contrasts experience higher moisture transports toward land areas. The reasons for increased temperature change contrasts between ocean and land air masses with global warming are complex and hence outside the scope of this study. Spatially inhomogeneous or regional radiative forcings however, may contribute to some of the observed variations. In Liepert and Previdi (2009) we suggested that the discrepancies noted in precipitation changes between models and observations at the end of the 20th century may be due to the various ways natural and anthropogenic aerosols are treated in IPCC-AR4 climate models. Here we use the same hypothesis for the moisture transport and show how spatially inhomogeneous, anthropogenic aerosols can effect atmospheric moisture transport in one model. Two special 20th century runs of the GISS-ER fully coupled model (prepared for IPCC-AR4) were used where anthropogenic forcings were introduced individually (see Hansen *et al* 2005). In this model version the global atmospheric moisture budget is almost balanced and no drift over time could be detected. The atmospheric moisture transports from oceans to land is calculated from outputs of the control (i.e., unforced) run, the 20th century anthropogenic greenhouse gases only run and of the 20th century anthropogenic aerosols (including direct, indirect, and semi-direct effect) experiments where the anthropogenic aerosol forcing is spatially and temporally non-homogeneous. The GISS model results lie well within the variability of the models shown in figure 3. The resulting atmospheric moisture transports from oceans to land in the 20th century are 0.90 Sv in the control run, 0.95 Sv in the GHG and 0.99 Sv in the anthropogenic aerosol experiment. The moisture transport to land areas increases by 0.13 Sv per 100 yr in the GHG and only by 0.06 Sv per 100 yr in the anthropogenic aerosol experiment. This is the case in spite of a similar sized, albeit opposite in sign, response of the surface radiative energy budget (Romanou *et al* 2007). The result suggests that the inclusion of spatially distinct aerosol distributions in climate models affect the atmospheric moisture transport from oceans to land differently than spatially homogeneous GHG forcings.

Furthermore, the analysis of the dry zone extension reveals large model-to-model variability as well. The differences in spatial pattern between model subsets with positive and negative moisture imbalances are comparable to the differences in the predicted pattern due to climate changes in the 21st century. Thus quantification of the pole-ward shifts of dry zones based on $E - P$ fields are dependent on the selection of models used for the analysis. Hence multi-model assessments should be evaluated with caution and other meteorological parameters as described above should be added to such an analysis. The current study has not addressed the possible causes of the biases, which is subject of future research and beyond the scope of the letter. Our overarching goal, however was investigating the self-consistency (Lucarini and Ragone 2011) of climate models in the CMIP3 archive and provide guidance for applying and improving the next generation on Earth system and climate models in CMIP5 and beyond.

Acknowledgments

The authors thank the reviewers and particularly V Lucarini for their insightful comments. The authors also thank the modeling groups for making their model output available for analysis, the Program for Climate Model Diagnosis and Inter-comparison (PCMDI) for collecting and archiving this data, and the WCRP's Working Group on Coupled Modeling (WGCM) for organizing the model data analysis activity. The WCRP CMIP3 multi-model dataset is supported by the Office of Science, US Department of Energy. This work was sponsored by NASA-MAP Program grant #NNG06GC66G and NSF Antarctic Oceans and Atmospheric Sciences grant #0944103. We thank Reto Ruedi, and Ken Lo for providing the NASA-GISS model simulations and the reviewers for their insightful comments.

References

Baumgartner A and Reichel E 1975 *The World Water Balance: Mean Annual Global, Continental and Maritime Precipitation, Evaporation and Run-Off* (Amsterdam: Elsevier)

Edwards J M 2007 Oceanic latent heat fluxes: consistency with the atmospheric hydrological and energy cycles and general circulation modeling *J. Geophys. Res.* **112** D06115

Gupta A 2007 *Large Rivers: Geomorphology and Management* (Chichester: Wiley)

Hansen J, Sato M and Ruedy R 1997 Radiative forcing and climate response *J. Geophys. Res.* **102** 6831–64

Hansen J *et al* 2005 Efficacy of climate forcings *J. Geophys. Res.* **110** D18104

IPCC-AR4 2007 *Contribution of Working Group I to the Fourth Assessment Report of the Intergovernmental Panel on Climate Change* ed S Solomon, D Qin, M Manning, Z Chen, M Marquis, K B Averyt, M Tignor and H L Miller (Cambridge: Cambridge University Press)

Kavetski D and Clark M P 2010 Ancient numerical daemons of conceptual hydrological modeling: 2. Impact of time stepping schemes on model analysis and prediction *Water Resour. Res.* **46** W10511

Liepert B G 2010 The physical concept of climate forcing *WIREs Clim. Change* **1** 786–802

Liepert B G and Previdi M 2009 Do models and observations disagree on the rainfall response to global warming? *J. Clim.* **22** 3156–66

Lucarini V, Danihlik R, Kriegerova I and Speranza A 2008 Hydrological cycle in the Danube basin in present-day and XXII century simulations by IPCCAR4 global climate models *J. Geophys. Res.* **113** D09107

Lucarini V and Ragone F 2011 Energetics of climate models: net energy balance and meridional enthalpy transport *Rev. Geophys.* **49** RG1001

Peixoto J P and Oort A H 1992 *Physics of Climate* (New York: American Institute of Physics)

Previdi M 2010 Radiative feedbacks on global precipitation *Environ. Res. Lett.* **5** 025211

Previdi M and Liepert B G 2007 Annular modes and Hadley cell expansion under global warming *Geophys. Res. Lett.* **34** L22701

Previdi M and Liepert B 2011 The vertical distribution of climate forcings and feedbacks from the surface to top of atmosphere *Clim. Dyn.* at press (doi:10.1007/s00382-011-1233-8)

Reichler T and Kim J 2008 How well do coupled models simulate today's climate? *Bull. Am. Meteorol. Soc* **89** 303–11

Rodríguez J, Johns T, Thorpe R and Wiltshire A 2011 Using moisture conservation to evaluate oceanic surface freshwater fluxes in climate models *Clim. Dyn.* **37** 205–19

Romanou A, Liepert B, Schmidt G A, Rossow W B, Ruedy R A and Zhang Y 2007 20th century changes in surface solar irradiance in simulations and observations *Geophys. Res. Lett.* **34** L05713

Schanze J J, Schmitt R W and Yu L L 2010 The global oceanic freshwater cycle: a state-of-the-art quantification *J. Mar. Res.* **68** 569–95

Seidel D J, Fu Q, Randel W J and Reichler T J 2008 Widening of the tropical belt in a changing climate *Nature Geosci.* **1** 21–4

Son S W *et al* 2008 The impact of stratospheric ozone recovery on the Southern Hemisphere westerly jet *Science* **320** 1486–9